



# Interface Damage in Titanium Dental Implant Due to Tribocorrosion: The Role of Mastication Frequencies

Maria F. Alfaro<sup>1</sup> · Peter K. Rossman<sup>2</sup> · Isabella da Silva Viera Marques<sup>1,3</sup> · Anirudh Dube<sup>4</sup> · Christos Takoudis<sup>2</sup> · Tolou Shokuhfar<sup>2</sup> · Mathew T. Mathew<sup>1,2,5</sup> · Cortino Sukotjo<sup>1,2</sup>

Received: 6 February 2019 / Revised: 17 July 2019 / Accepted: 18 July 2019 / Published online: 8 August 2019  
© Springer Nature Switzerland AG 2019

## Abstract

The aim of this study was to investigate the influence of fretting motions on the depassivation–repassivation processes occurring in Ti6Al4V alloy, at an in vitro simulated oral environment. Ti6Al4V discs were subjected to fretting–corrosion using a pin-on-disc tribometer. Specimens underwent 2000 motion cycles, with  $\pm 500 \mu\text{m}$  of fretting stroke, and 8 N of load at frequencies of 1, 2, and 4 Hz. Surface characterization was performed using white-light interferometry and scanning electron microscope. Total mass loss ( $K_{\text{wc}}$ ), and mass loss due to wear ( $K_{\text{w}}$ ) and corrosion ( $K_{\text{c}}$ ) were calculated. Lower potentials were reached at a frequency of 4 Hz. The coefficient of friction was statistically higher ( $p > 0.05$ ) under 1 Hz ( $\mu = 0.66$ ) as compared to that of 2 and 4 Hz ( $\mu = 0.53$ ;  $\mu = 0.51$ ).  $K_{\text{wc}}$  was significantly higher ( $p < 0.001$ ) on specimens subjected to a higher frequency of 4 Hz (16.1  $\mu\text{g}$ ), when compared to 1 and 2 Hz (0.30  $\mu\text{g}$ ; 1.24  $\mu\text{g}$ ). Under mechanical input, titanium's oxide layer is constantly removed and reformed involving two processes called depassivation and repassivation. This study was conducted as a way to understand the influence of the mechanical stimuli alongside the oxide layer stability. The mechanical and chemical attacks encountered by Ti6Al4V vary regarding the fretting frequency applied. Lower fretting frequencies allow for the better chance of repassivation resulting in a protective barrier against degradation processes.

**Keywords** Fretting–corrosion · Dental implants · Micromotion · An oxide layer · Ti6Al4V

## 1 Introduction

In dentistry, the usage of dental implants is highly successful; however, early failure, undesirable pain, and the presence of infections are common downfalls that constantly invade this field. Dental implant failures are subjected to a wide list of multifactorial aspects including biological, chemical, and mechanical aspects [1, 2].

Titanium and its alloys are well known for its biocompatibility, which is enhanced by the presence of a stable protective oxide film [3]. This oxide layer, mainly consisting of amorphous titanium dioxide ( $\text{TiO}_2$ ), constantly forms on the outer surface of the metal once in contact with oxygen in a process called passivation [4–9]. However, this ~4 to 5 nm thickness of titanium oxide film presents limited strength when exposed to certain mechanical and electrochemical situations [4, 9]. Once this layer is disrupted, the bulk metal is exposed and a consequent metallic breakdown will occur. Furthermore, the presence of these released substances might cause a harmful effect around the peri-implant tissue compromising the final implant outcome [10, 11].

Cyclic occlusal loading will take place during normal masticatory activity inducing mobility of the joint components contained by dental implants [12]. Such a biomechanical event may be enhanced in the presence of parafunctional habits (i.e., bruxism), due to a continuous overloading activity faced by these devices and their correspondent superstructure [13]. The generated micro-movements are likely to occur at the implant–bone interface as well as within the

✉ Mathew T. Mathew  
mtmathew@uic.edu

<sup>1</sup> Department of Restorative Dentistry, University of Illinois at Chicago College of Dentistry, Chicago, IL, USA

<sup>2</sup> Department of Bioengineering, University of Illinois at Chicago, Chicago, IL, USA

<sup>3</sup> Department of Prosthodontics and Periodontology, University of Campinas (UNICAMP), São Paulo, Brazil

<sup>4</sup> Ducom Tribology Limited, Bangalore, India

<sup>5</sup> Department of Biomedical Science, UIC School of Medicine, Rockford, IL, USA

interior implant component (abutment, screw, and crown) interfaces [14]. This process of accelerated surface damage taking place at the interface of contacting materials subjected to low amplitude oscillatory movements is commonly known as fretting [15].

The wear process present in dental implant devices does not occur on its own; rather it is very common accompanied by corrosion activity due to the presence of saliva and other physiological fluids commonly found in the oral environment. This synergistic role in both mechanical and electrochemical processes present in metallic biomaterials leads to the development of bio-tribocorrosion systems (fretting–corrosion, sliding–corrosion, crevice–corrosion, etc.) which have been found to represent an important concern for implant applications as shown in Fig. 1 [5, 6, 15–18].

So far multiple oral environmental factors (food, saliva, bacterial biofilm, pH changes, and systemic conditions) that influence the mechanical–corrosion mechanisms in bio-compatible metals have been studied [16, 19–23]. Overall, under tribocorrosion tests an inferior corrosion resistance was shown in the presence of fluorides, bacteria, and low pH levels, pointing out the resultant less protective oxide film in materials such as Cp Ti and Ti6AL4V [5, 7, 16].

In addition, parameters such as fretting frequency, track length, and applied load will impact the fretting–corrosion behavior in biomaterials [24]. Many studies conducted in modular hip prosthesis interfaces have highlighted the influence of various fretting regimes affecting the oxide layer's integrity and its influence on the overall implant alloy degradation [25–28]. However, only a few studies have been published regarding fretting–corrosion mechanisms in dental implant systems [7, 15, 29]. Therefore, due to the dynamics encountered under masticatory activity, there is a need to understand how mechanical parameters influence the oxide film disruption and its subsequent repassivation process on

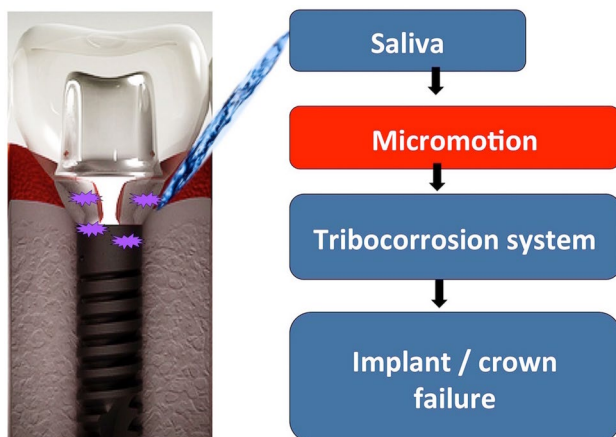


**Fig. 1** Schematic diagram of the tribocorrosion phenomenon in dental implant systems

titanium substrates. The obtained information will be critical for the long-term performance of the currently used dental devices.

The goal of this study was to explore the role of fretting frequencies in the depassivation and repassivation processes occurring in titanium dental implant's alloy (Ti6Al4V) in a fretting–corrosion-simulated oral environment. Different fretting frequencies (1, 2, and 4 Hz) were tested in each of the specimens using a pin-on-disc tribometer system coupled with a potentiostat. Free potential, potentiostatic, and potentiodynamic tests were performed. It was hypothesized that as the fretting frequency is increased, the process of passive film removal happening in Ti6Al4V alloy increases enhancing both mechanical and chemical degradations.

## 2 Materials and Methods

### 2.1 Specimens and Solution

A total of 21 Ti6Al4V discs of 15.0 mm in diameter and 2.0 mm thick were used (Mac-Master Carr, Elmhurst, IL, USA). The sample discs were polished following the standard metallographic methods until mirror surface finishing. Once the specimens were properly mounted into an acrylic resin base (Caulk Orthodontic Resin, Denstply), they were wet-ground with 240–800 grit sandpapers (Carbimet 2, Buehler, Lake Bluff, IL, USA). Afterwards, a microfiber cloth (TextMet Polishing Cloth, Buehler) was used along with a diamond paste (MetaDi 9-micron, Buehler) and a lubricant (MetaDi Fluid, Buehler) before moving on to the final step, which was performed with a chemomet polishing cloth (Chemomet I, Buehler) and colloidal silica suspension (MasterMed, Buehler) alternated with distilled water. After the polishing procedure, all samples were taken off the resin and sonicated in 70% isopropanol for 15 min. A zirconium oxide pin with a circular contact area of  $\sim 7 \text{ mm}^2$  was used as the correspondent contact opponent. This pin was polished and cleaned with an 800 grit polishing cloth (Carbimet 2, Buehler) and isopropanol 70%, respectively, before and after every test.

The electrolyte was artificial saliva with pH of 6.0, to mimic the oral conditions. The composition of the electrolyte was based on Fusayama and Meyer's solution [5] listed in Table 1.

### 2.2 Tribocorrosion Test Protocol

All tests were performed using a linear reciprocating tribometer (DUCOM Instruments, Bohemia, New York, USA) coupled with a potentiostat (SP-240 Bio-Logic, LLC, Knoxville USA). Figure 2 shows the schematic setup of the tribocorrosion apparatus. A pin-on-disc tribo-system was used, with

**Table 1** Fusayama and Meyer’s artificial saliva composition

Component	Concentration (g/L)
KCl	0.4
NaCl	0.4
CaCl·2H <sub>2</sub> O	0.906
NaH <sub>2</sub> PO <sub>4</sub> ·2H <sub>2</sub> O	0.690
Na <sub>2</sub> S·9H <sub>2</sub> O	0.005

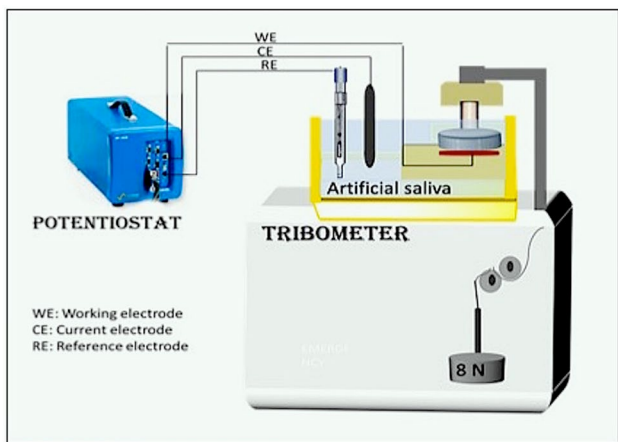


**Fig. 2** Schematic of tribocorrosion (fretting–corrosion) experimental setup

a counter contact pin made of zirconium oxide. The total number of reciprocating cycles was fixed as 2000 cycles (simulating daily masticatory activity), with varied fretting

frequencies (1, 2, and 4 Hz), a constant load of 8 N, and a mean Hertzian pressure of 0.91 MPa (this is only a representative value from the mastication cycle). In order to simulate fretting motion, the stroke length of 1 mm ( $\pm 500 \mu\text{m}$ ) was achieved.

The tribometer was interfaced with the potentiostat, and the experiments were performed using the standard three-electrode cell system [6]. A saturated calomel electrode (SCE) was used as the reference electrode (RE), a graphite rod as the counter electrode (CE), and a specimen copper electrode placed underneath the sample function as a working electrode (WE). In this study, the tribocorrosion experiments were conducted in three modes: (1) potentiodynamic mode, (2) free potential mode, and (3) potentiostatic mode at  $-0.25 \text{ V}$  (vs. SCE) (Fig. 3).

In the potentiodynamic experiments, after the initial open circuit potential measurements, the samples were anodically polarized from  $-0.8$  to  $1.8 \text{ V}$  at a scan rate of  $5 \text{ mV s}^{-1}$ . In the case of free potential and potentiostatic modes, the testing protocol consisted of three phases: an initial stabilization, a fretting–corrosion testing, and a final stabilization (Fig. 4). After the discs were held firmly in the tribocorrosion cell, the initial stabilization started with an electrochemical-cleaning phase at a constant voltage of  $-0.9 \text{ V}$ . Consequently, the samples underwent an open circuit potential (OCP), followed by electrochemical impedance spectroscopy (EIS) measurements at a range from  $100 \text{ kHz}$  to  $5 \text{ mHz}$  with a  $10 \text{ mV}$  of scan amplitude. After finishing these first steps, the samples underwent the fretting process. The coefficient of friction, the potentials, and current was monitored during the fretting stage. After the fretting stage, the pin was released and the final stabilization was conducted. When

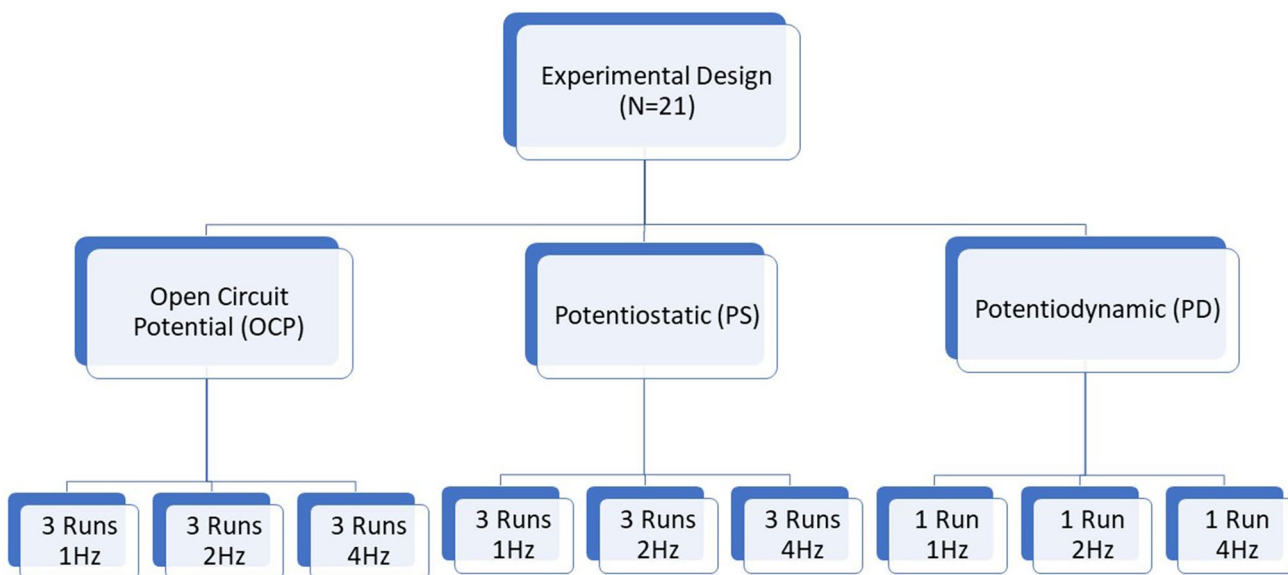


**Fig. 3** Experimental design

I. Initial Stabilization				II. Fretting Corrosion Testing			III. Final Stabilization	
				1) Free Potential 2) Potentiostatic				
OCP	Cleaning	OCP	EIS 1	Apply Load	Fretting	Remove Load	EIS 2	OCP
180 s	300 s	1800 s	100kHz-5mHz	600 s ↓ 600 s	1Hz:2000s 2Hz:1000s 4Hz:500s	600 s ↓ 600 s	100kHz-5mHz	1800 s
I. Initial Stabilization				II. Fretting Corrosion			III. Final Stabilization	
				1) Potentiodynamic				
OCP	Cleaning	OCP Apply Load	Fretting During Cyclic Polarization			OCP Remove Load		
180 s	300 s	600s ↓ 600s	1 Hz 2 Hz 4 Hz			600 s ↓ 600s		

Fig. 4 The standard protocol used during fretting–corrosion testing for free potential, potentiostatic, and potentiodynamic modes. *OCP* open circuit potential, *EIS* electrochemical impedance spectroscopy

the experiment was over, the samples were removed from the electrochemical cell, and a 15-min sonication in 70% isopropanol was performed before storage.

### 2.3 Surface Characterization

Surface characterization was performed for visual analysis of the worn and corroded surface scars by the scanning electron microscopy (SEM, Joel JSM-6490 LV, Japan). In order to estimate the total mass loss ( $K_{wc}$ ) reached during the tribocorrosion interaction, a white-light interferometry microscopy (Zygo New View 6300, Middlefield, CT) was used to determine the total volumetric loss encountered by each specimen. Furthermore, the alloy’s density (4.43 g/cm<sup>3</sup>) was considered in order to obtain the total mass loss. The mass loss due to corrosion ( $K_c$ ) values was estimated using the Faraday’s Law equation [5]. Those values were then subtracted from the total mass loss due to wear and corrosion in order to find out the mass loss due to wear ( $K_w$ ):

Simple model equation

$$K_{wc} = K_w + K_c, \tag{1}$$

$$K_w = K_{wc} - K_c. \tag{2}$$

Faraday’s law equation

$$K_c = \frac{Mit}{ZF}, \tag{3}$$

where  $K_c$  is the mass loss due to corrosion,  $M$  the atomic mass,  $I$  the total current,  $t$  the exposure time,  $Z$  the number of electrons passed in corrosion reaction (assumed to be 2), and  $F$  is the Faraday’s constant (96,500 C/mol).

### 2.4 Statistical Analysis

The coefficient of friction, total mass loss ( $K_{wc}$ ), mass loss due to corrosion ( $K_c$ ), and mass loss due to wear ( $K_w$ ) were statistically analyzed using one-way analysis of variance (ANOVA) as a way to analyze the significant difference among the applied frequencies of 1, 2, and 4 Hz used during the tribocorrosion testing. Tukey’s HSD (Honest Significance Difference) test was used as well for the multiple-comparison technique when needed. A mean difference significant at the 0.05 level was used for all tests (Statistical Package for Social Sciences, version 17.0; SPSS Inc, Chicago, IL USA).

### 3 Results

#### 3.1 Potentiodynamic Curves

Representative potentiodynamic polarization curves for each group were attained at the same time as mechanical activity was induced, and the results are shown in Fig. 5.

A cyclic curve for Ti6Al4V without motion was also incorporated into the graph as a representative example. A clear difference can be seen in the trend followed by the curves when the specimens underwent fretting motion. Without fretting, the electrochemical polarization curve for Ti6Al4V follows the typical anodic, cathodic, and passivation regions according to studies previously published [5, 16]. The curve appears without fluctuations due to the absence of mechanical motion. At positive potential, a passive plateau can be observed suggesting the formation of a stable oxide layer.

Specimens under the three different applied frequencies exhibited a similar fluctuating pattern throughout the cycle. However, as the frequency is increased, a higher current density is achieved. Samples undergoing a fretting frequency of 4 Hz display a greater shift to the right, in contrast with frequencies of 1 Hz and 2 Hz in which only a slight increase in current is observed.

#### 3.2 Open Circuit Potential Data and Coefficient of Friction (COF)

An open circuit potential that was recorded before, during, and after the fretting process is shown in Fig. 6a, with its correspondent coefficient of friction values (Fig. 6b, c).

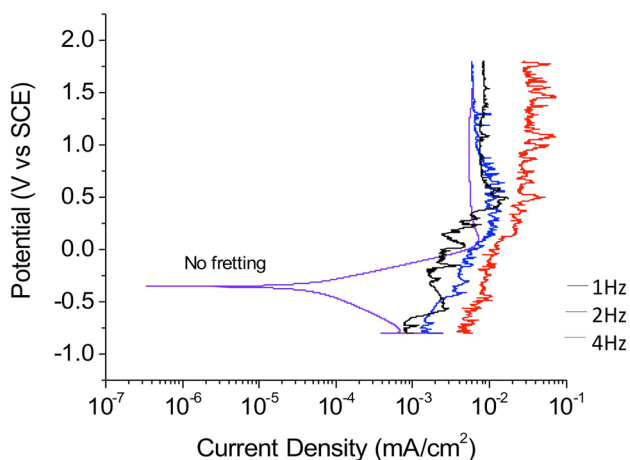


**Fig. 5** Potentiodynamic polarization curves for Ti6Al4V during fretting–corrosion tests at frequencies of 1, 2, and 4 Hz. A curve without fretting activity was added as a representative example

In all conditions, an abrupt drop in potential is clearly seen by the time the fretting is started at approximately 4560 s with a concomitant increase in the friction values. While fretting, repeatedly fluctuations in potential are observed, following a gradual increase once the fretting stops.

At the applied frequency of 4 Hz, lower potentials (more negative) are reached when the fretting starts, in contrast with specimens fretted at frequencies of 1 Hz and 2 Hz. While fretting, the variations achieved in potential represented by the peak pattern are directly proportional to the applied frequency. Intense fluctuations are observed in specimens following a 4-Hz regimen, when compared with samples fretted at 1 Hz in which the oscillatory pattern seems to display shorter periods of voltage stabilization. Nevertheless, once the fretting motion is finished, a faster and higher shift into anodic potentials is observed at 4 Hz.

Regarding the coefficient of friction, an immediate rise in the values is observed once the fretting starts, with the presence of noticeable oscillations throughout the entire cycle. Among the groups, the coefficient of friction was higher for the frequency of 1 Hz (0.66) when compared to the other fretting frequencies of 2 and 4 Hz (0.53 and 0.51, respectively), and the difference was statistically significant ( $p < 0.05$ ).

#### 3.3 Evolution of Current Under Potentiostatic Tests

The evolution of current for each applied frequency was taken from potentiostatic tests performed at  $-0.25$  V. This potential corresponds to the  $E_{\text{corr}}$  values for Ti6Al4V obtained at the potentiodynamic curves without fretting, Fig. 5. The evolved current obtained during the fretting stage for each applied frequency over time is seen in Fig. 7. Overall, an increase in the current flow can be appreciated while the fretting mechanism takes place.

Differences in current are clearly observed as a function of the applied frequencies. Samples subjected to a frequency of 4 Hz display the highest current evolution among all three groups. In contrast, specimens subjected to the lowest applied frequency demonstrate a significantly lower current evolution, very close to zero.

#### 3.4 Mass Loss Measurements

The correspondent mass loss calculations for each applied frequency were obtained according to Eqs. (1–3). The results obtained are shown in Table 2.

According to the graphs shown in Fig. 8a–c, it can be seen that more mass loss due to corrosion, wear, and the combined wear–corrosion mechanisms occur when Ti6Al4V discs are subjected to a higher fretting frequency of 4 Hz. These results are statistically significant among



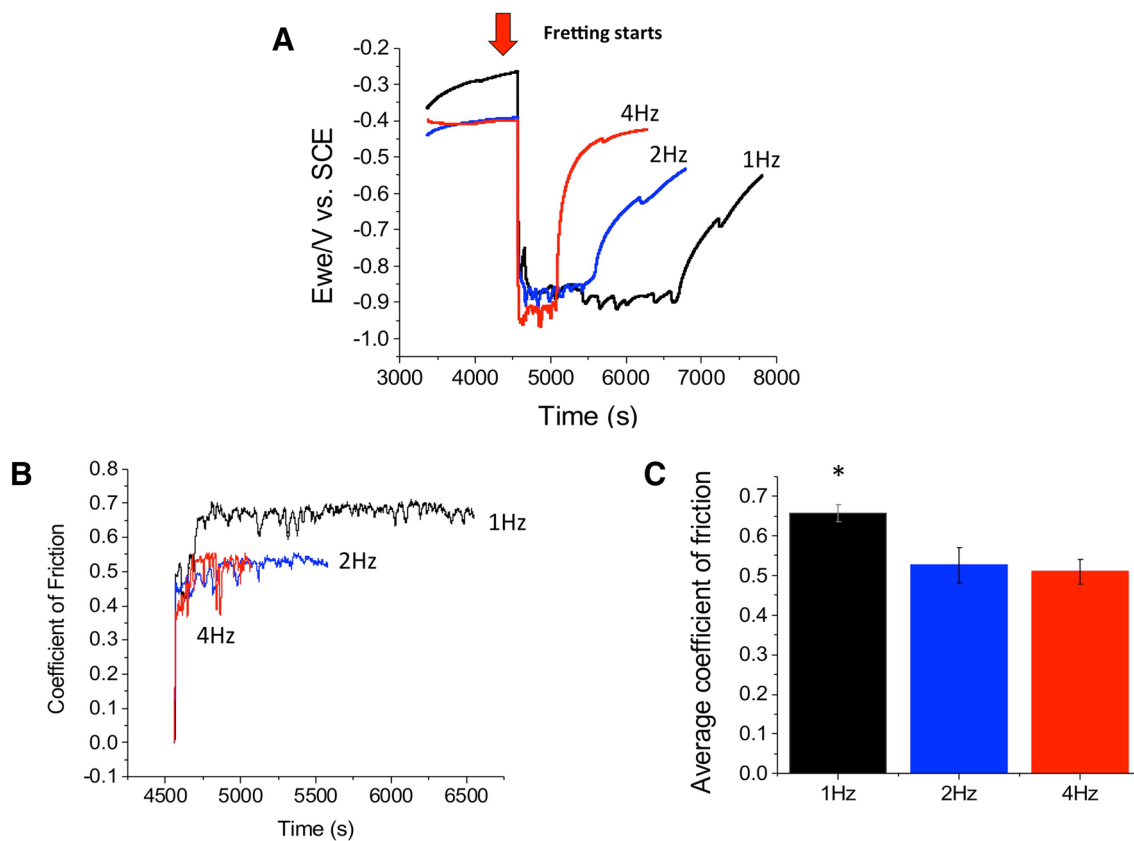


**Fig. 6** a OCP evolution versus time during fretting activity of zirconium oxide pin against Ti6Al4V alloy discs at the three applied frequencies. b Evolution of the friction coefficient during 2000 fretting

cycles at each applied frequency. c Average of the coefficient of friction values at 1, 2, and 4 Hz. \*Shows significant difference ( $p < 0.05$ )

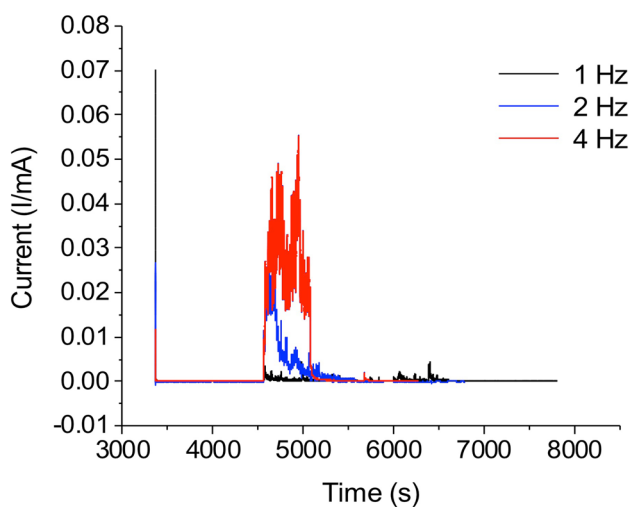


**Fig. 7** Current evolution versus time obtained during potentiostatic tests (-0.25 V). The values were recorded before, during, and after fretting motions at the three different applied frequencies

**Table 2** Weight loss distribution for the three different applied frequencies: total weight loss ( $K_{wc}$ ), weight loss due to corrosion ( $K_c$ ), and weight loss due to wear ( $K_w$ )

Mass loss distribution				
Frequency	$K_{wc}$ ( $\mu\text{g}$ )	$K_c$ ( $\mu\text{g}$ )	$K_w$ ( $\mu\text{g}$ )	$K_c/K_w$
1 Hz	0.30 ( $\pm 0.01$ )	0.01 ( $\pm 0.01$ )	0.29 ( $\pm 0.02$ )	0.03 ( $\pm 0.01$ )
2 Hz	1.21 ( $\pm 0.83$ )	0.15 ( $\pm 0.08$ )	1.99 ( $\pm 0.43$ )	0.07 ( $\pm 0.04$ )
4 Hz	16.1 ( $\pm 2.72$ )	0.59 ( $\pm 0.19$ )	15.5 ( $\pm 2.89$ )	0.04 ( $\pm 0.01$ )

$K_{wc}$  total mass loss,  $K_c$  mass loss due to corrosion,  $K_w$  mass loss due to wear,  $K_c/K_w$  synergistic ratio

the three groups ( $p < 0.001$ ). The least amount of degradation takes place at a fretting frequency of 1 Hz; however, no significant difference is shown when compared with specimens exposed to frequencies of 2 Hz. Additionally, as seen in Fig. 8a, the mass loss values attributed to electrochemical oxidation appear to be lower than the ones attributed to pure wear mechanisms.

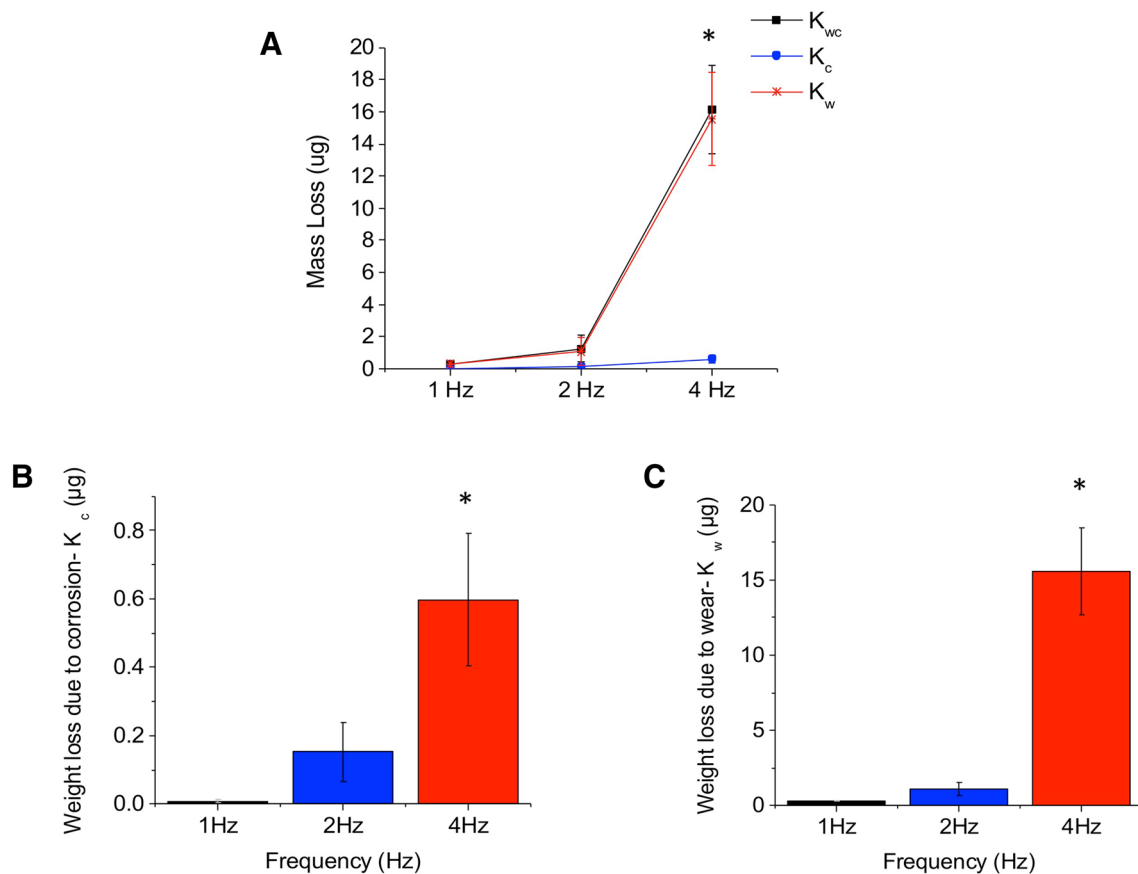


**Fig. 8** **a**  $K_{wc}$ ,  $K_c$ , and  $K_w$  averages obtained at each of the tested fretting frequencies. **b** Evolution of  $K_c$  as a function of fretting frequencies, **c** evolution of  $K_w$  as a function of fretting frequencies. \*Shows significant difference ( $p > 0.001$ )

### 3.5 Surface Characterization

The wear scar obtained in each specimen was evaluated using scanning electron microscopy (SEM) and white-light interferometry (WLI). Overall, the mechanical affection in Ti6Al4V surfaces happened to be worse when the motion frequency was increased giving rise to an incremental plastic deformation.

The relevant SEM images of the wear scars obtained after tribocorrosion testing for the three different fretting frequencies considered above are presented in Fig. 9. Among all the groups, the wear track is characterized by striations following the direction of the movement with the presence of material detachment at the fretting area. However, different patterns can be seen as a function of the fretting frequency. At lower fretting frequencies of 1 Hz, less damage is observed, with the presence of isolated wear debris acting as third-body particles (Fig. 9a–c). Additionally, a more affected surface is present when the fretting occurs at a frequency of 2 Hz displaying an increased abrasive surface, with exposure of multiple clear and dark striations showing corrosion pits (Fig. 9d–e). For the highest applied frequency of 4 Hz, the suffered mechanical

damage becomes more evident, and it is shown in Fig. 9g–i. There is the presence of well-defined grooves and wider cracks. The manifestation of detached flakes suggesting an ongoing degradation process of the metallic surface is also shown.

The most representative WLI images for each applied frequency are presented in Fig. 10. In general, at lower applied frequencies, less delimited wear scars are observed. The discs that underwent fretting motion at frequency 1 Hz show shallower wear scars, demonstrating less surface damage (Fig. 10a). Furthermore, as seen in Fig. 10b, Ti alloy's discs fretted at 2 Hz display a heavily damaged central zone with an external area of spread material. Ultimately, a concise and delimited wear scar with severe material degradation at the central part is visualized on the discs subjected to a fretting frequency of 4 Hz (Fig. 10c).

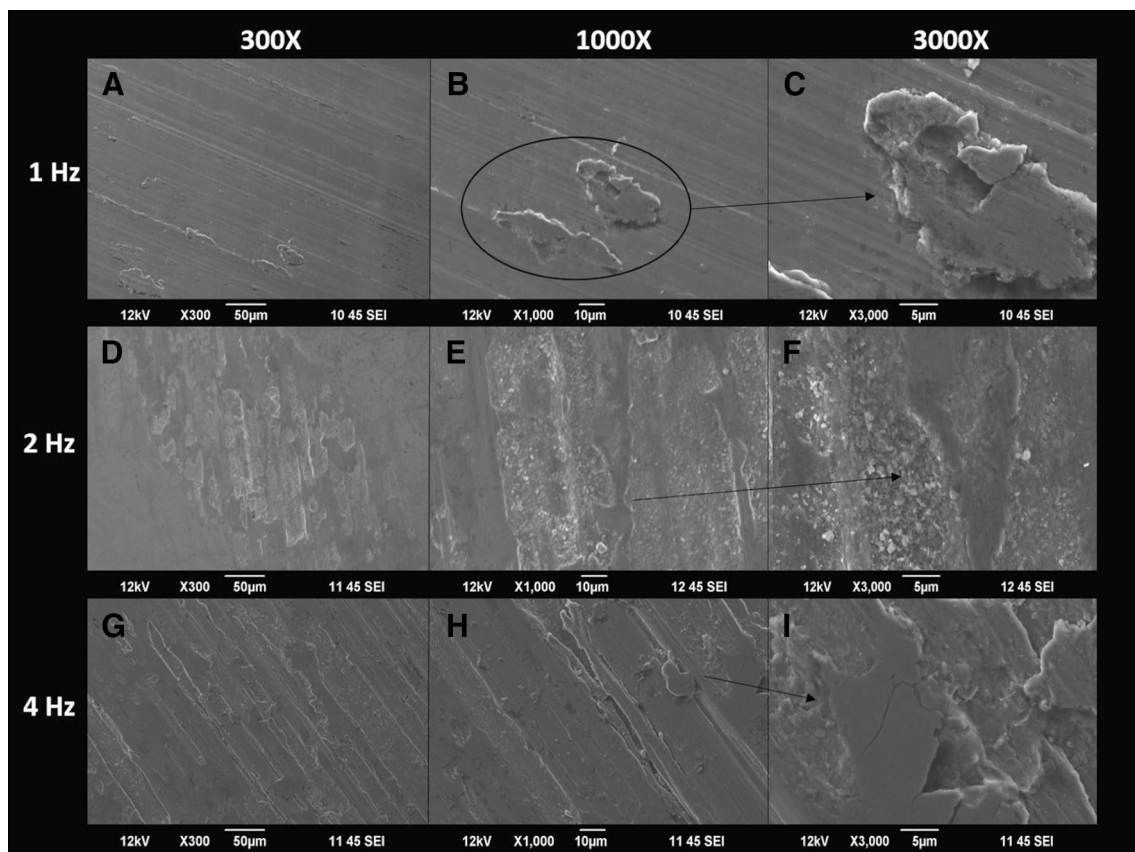


**Fig. 9** SEM images of the worn areas of Ti6Al4V alloy discs after fretting–corrosion experiments. **a** Frequency of 1 Hz with 300× magnification. **b** Frequency of 1 Hz with 1000× magnification. **c** Frequency of 1 Hz with 3000× magnification. **d** Frequency of 2 Hz with

300× magnification. **e** Frequency of 2 Hz with 1000× magnification. **f** Frequency of 2 Hz with 3000× magnification. **g** Frequency of 4 Hz with 300× magnification. **h** Frequency of 4 Hz with 1000× magnification. **i** Frequency of 4 Hz with 3000× magnification

## 4 Discussion

### 4.1 The Effect of Fretting Frequencies on the Fretting–Corrosion Behavior of Ti6Al4V Alloy

This study shows how the mechanical disruption of the inherent Ti-oxide layer (passive film) taken place at different fretting frequencies influences Ti6Al4V alloy's degradation.

Overall, under wear–corrosion conditions, a change in both corrosion and tribological features is likely to occur [30]. The obtained cyclic polarization curves (Fig. 5) show evidence of abundant oscillations demonstrating an irregular passivation region caused by the fretting motion applied at the surface of each titanium alloy disc. Specimens exposed to frequencies of 1 and 2 Hz exhibit superior corrosion behavior, due to the fact that lower current densities were reached [19].

Furthermore, it is known that the current density estimated from the potentiodynamic curves is proportional to the alloy's dissolution [31]. As for the samples exposed to a

frequency of 4 Hz, greater current densities were attained. This might be correlated with the presence of an interrupted passive film formation, which leads to a less protective oxide barrier.

### 4.2 Potential Evolution as a Function of Frequency

Additionally, as established in other studies, the variations in the open circuit potential (Fig. 6) indicate the presence of electrochemical processes occurring within the material's interface under the fretting tests [25]. A sudden drop in potential is achieved once the alloy's surface faces mechanical motion, indicating the onset of wear. This potential will then return back to more positive values as soon as fretting process stops [32]. Lower potential was reached at a higher applied frequency revealing more aggressive destruction of the protective oxide film with consequent exposure of the bulk alloy to the artificial saliva causing a subsequent decrease in the corrosion potential [30].

Perhaps when the discs subjected to the rubbing motion at higher frequencies, a more interrupted/accelerated



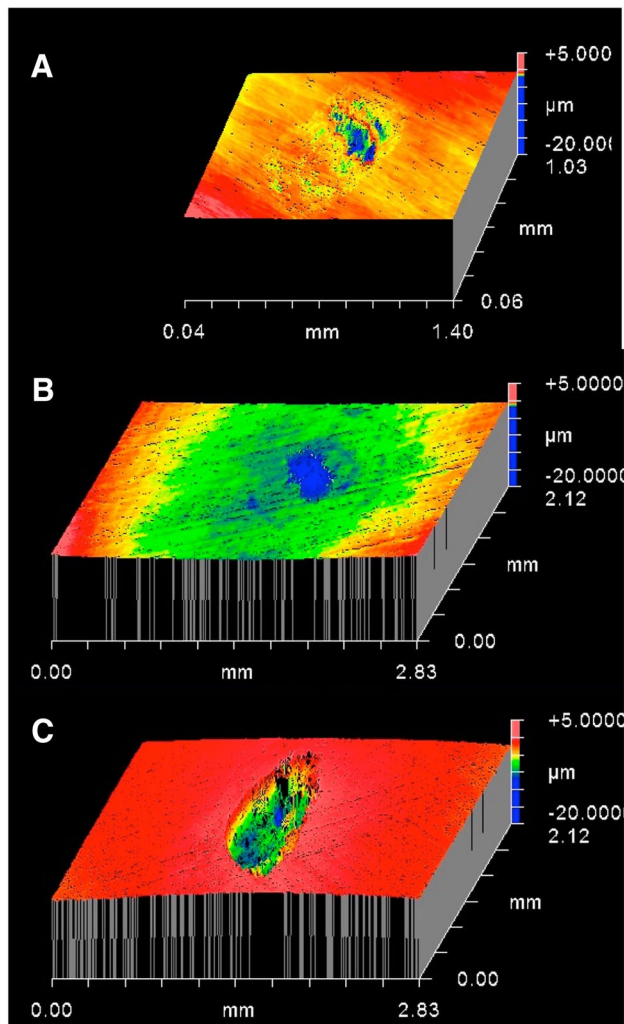


**Fig. 10** White-light interferometry 3D images of Ti6Al4V alloy discs after fretting–corrosion experiments. X and Y axes are in mm, and Z axes in  $\mu\text{m}$ . **a** Ti6Al4V alloy surface fretted at a frequency of 1 Hz. **b** Ti6Al4V alloy surface fretted at a frequency of 2 Hz. **c** Ti6Al4V alloy surface fretted at a frequency of 4 Hz

repassivation process might occur due to the continuous contact of the pin against the oxide layer and underneath the substrate. During 1 Hz frequency, the removable rate of the protective passive film seems to be slower than the one from the other two frequencies creating a more disperse fluctuation that shows long periods of depassivation and subsequent repassivation.

Regarding the coefficient of friction data, the sudden increase that was obtained during the initial period of fretting corresponds to the initial removal of the crushed and smeared debris from the coupled contacting surfaces [18]. The possibility of higher repassivation periods taking place at a fretting frequency of 1 Hz could lead to a vast presence of oxide layer fragments that may explain the increase in the movement's resistance [33]. This activity will result

in cumulative third-body particles trapped between the interfaces of the two rubbing surfaces [18]. In contrast, at the highest applied frequency of 4 Hz these particles were perhaps most likely pushed away from the contact area as the movement continues and thus showing the lower coefficient of friction values [34]. As the friction is the result of surface interactions at the tribological contacts, the higher values indicate the severe process at 4 Hz than other lower frequencies. The severity at the tribological contact could be resulted from the mechanistic transitions as the rubbing process is faster at 4 Hz frequencies, as explained above.

During the mechanical activity performed at an applied voltage of  $-0.25$  V, local destruction of the protective passive layer takes place (depassivation) exposing the bare surface of the alloy to the former electrolyte. This process will lead to an increase in metallic dissolution resulting in higher current values [33]. According to Mischler et al. [35], mechanisms such as passive film detachment, surface plastic deformation, incorporation of abrasive debris, and former loss of metallic particles are involved in this process. This behavior will basically suggest an increase in Ti alloy's surface damage and a higher release of metal ion/debris to the surrounding media [5].

### 4.3 Current Variation as a Function of Frequency

The current fluctuations observed during the potentiostatic tests shown in Fig. 5 can be correlated to a continuous depassivation and repassivation activity experienced on the surface of the alloy [5, 33, 35]. The obtained results suggest that there is a less interrupted repassivation process when tribological motions take place at a frequency of 1 Hz experiencing fewer alloy's dissolution.

On the other hand, a more deteriorated and deficient passive film can be expected when specimens are exposed to higher frequencies. At a fretting frequency of 4 Hz, an uninterruptedly oxide film removal less capable to recover could be correlated with the current evolution obtained results.

It is well known that titanium's oxide film has a lubricating nature that will tend to reduce the wear rate [32]. The oxide layer thickness can be increased as a result of repeated removal and reformation process [36]. According to Masmoundi et al. following passivation, a passive film can increase 10 times its regular thickness [36]. The newly formed oxides are normally harder than the virgin titanium alloy [24]. In agreement to what was written before, the experimental samples fretted at a frequency of 1 Hz resulted in higher material resistance against chemical and mechanical events.

As the fretting frequency is increased, a shorter period of time is available for the repassivation process to occur. Regardless of the rapid and continuous oxide layer formation rate, titanium alloy's oxides can be easily fragmented

and worn away with almost no possibility of adherence to the alloy's surface. Therefore, their protective ability against metallic degradation will be diminished and will lead to a severe wear process [37].

The mass loss process faced by Ti6Al4V specimens (Fig. 8) is characterized by its exponential increase proportional to the applied frequency. In other words, experiencing the same number of fretting cycles, specimens that were subjected to motion frequencies of 4 Hz show the highest material degradation. This phenomenon could be attributed to the interrupted repassivation activity presented at this frequency, which will lead to a less protective passive layer on top of the alloy's surface [33]. Without a stable oxide layer, titanium and its alloys will be corroded/degraded in the same way as other non-passive metals. Such results are also correlated with the evolved current density obtained during the fretting phase. With that being said, it can be stated that the overall degradation of Ti6Al4V alloy closely depends on the stage of its passive film. The oxide layer will not only protect the metal from the corrosion attack but will also have an important role in the mechanical wear resistance.

#### 4.4 Evidence from Worn Surfaces and Possible Fretting–Corrosion Mechanisms

The worn surfaces are shown in SEM and WLI images (Figs. 9, 10) analyzed after 2000 fretting cycles can be correlated with the results obtained for mass loss measurements and current evolution. For all groups, the presence of multiple striations suggests evidence of a predominant abrasive behavior [33]. The vaguely wear volume loss of Ti6AlV discs subjected to frequencies of 1 Hz may be attributed to the corrosion and mechanical protection afforded by the passive film [18]. The higher chance of repassivation taking place at the fretting mechanism of 1 Hz of frequency will contribute to the passive layer protectiveness [33].

The extended smearing layer shown in the specimens subjected to frequencies of 1 and 2 Hz could be the result of the spread wear debris generated during the mechanical activity [5, 16]. At these lower fretting frequencies, the wear scar pattern could be related to a micro-fragmentation of fine oxide particles [38].

Once the frequency is increased, the fracture and particle detachment will be increased as well. On the discs fretted at 4 Hz, a deeper wear track predominantly in the central part is observed in the WLI images. According to previous studies, a more pronounced depassivation activity with a high current evolution is more likely linked with particle detachment rather than with crushing of debris [34]. Moreover, an increased counter body penetration with continuous surface damage potentiated by a deficient passive film formation is also expected at higher fretting frequencies [34].

The fragments produced by wear processes appear to be different for each of the fretting frequencies, suggesting a predominance of oxide particles at the lower frequency regimes and full metallic particles at the highest ones [38]. These fragments may be generated by a micro-fragmentation process of the oxide debris and a degradation process of the bulk metallic structures [38].

#### 4.5 Synergism Between Fretting and Corrosion

As a way to determine the magnitude of the synergism between wear and corrosion, a  $K_c/K_w$  ratio was calculated as seen in Table 3 following the criteria proposed by Stack et al. [39].

The ratio values of  $K_c/K_w$  among all groups range from 0.03 to 0.07 ( $p=0.353$ ; ANOVA). Since the obtained results lie between 0.1 and 1, the resultant of a dominant wear–corrosion mechanism is indicated according to various tribocorrosion studies [5, 16, 40]. A clearly marked influence of the mechanical wear is demonstrated in this fretting–corrosion study especially on the discs fretted at higher frequencies, which is in agreement with the results previously discussed.

In general, the interplay of corrosion and wear activities will have an important influence on Ti6Al4V alloy's outcome. However, this complex degradation process will be enhanced by the mechanical stimuli in the presence of inferior protection assumed by a compromised oxide layer [33, 40]. Not only an improvement in the mechanical properties of the material is needed in order to reduce titanium's overall degradation, but also a more stable and protective oxide layer could be beneficial [38].

#### 4.6 Clinical Significance

The protective oxide layer formed when titanium dental implants are placed in the oral cavity can easily break apart when subjected to mechanical input such as normal masticatory activity. In the present study, a titanium alloy (Ti6Al4V) commonly used for dental abutments was tested at different fretting frequencies. This was conducted as a way to understand if the variability of the mechanical stimuli had a significant influence in the metal's oxide layer and how detrimental this could be. It was shown that at a frequency of 1 Hz there is still the presence of mechanical and electrochemical

**Table 3** Synergistic ratio proposed by Ref. [39]

Ratio value ( $K_c/K_w$ )	Degradation mechanism
$K_c/K_w < 0.1$	Wear
$0.1 \leq K_c/K_w < 1$	Wear–corrosion
$1 \leq K_c/K_w < 10$	Corrosion–wear
$K_c/K_w > 10$	Corrosion

resistance due to a better chance of repassivation, in contrast with results obtained at the highest applied frequency of 4 Hz. In addition, this layer showed to have a positive effect not only alongside the electrochemical oxidation but also on the mechanical attack.

The occlusal activity at which the dental implant systems are exposed could be determinant regarding their degradation and longevity. Additionally, the occlusal forces faced by dental implant patients are multidirectional, with the existence of various intensities and frequencies especially in the presence of parafunctional habits. With this being stated, a thorough occlusal analysis with a pertinent treatment plan should be taken into consideration when restoring dental implants.

Further investigations resembling a more accurate clinical environment should be performed. A fretting–corrosion setup using actual dental implant components with the correspondent incorporation of smaller amplitude strokes and multidirectional mechanical parameters is encouraged.

## 5 Conclusions

Mechanical disturbances encountered at different fretting frequencies were used in order to investigate how variations within depassivation and repassivation processes may influence the protective features of Ti6Al4V oxide layer against mechanical and chemical degradation. The following conclusions can be highlighted based on the outcomes shown in this study:

- Under both wear and corrosion conditions, Ti6Al4V alloy mainly degraded by mechanical wear mechanisms, independently of the fretting frequencies in this study.
- The total mass loss experienced in Ti6Al4V alloy specimens was higher when the fretting frequencies were increased.
- The higher chance of repassivation observed at the lower applied frequencies will result in a protective barrier against electrochemical and mechanical attacks.
- The constantly removed oxide debris acting as third-body particles tend to increase the friction coefficient at the lower applied frequency of 1 Hz. As the frequencies increase, these particles are most likely pushed away from the wear track decreasing the friction values.
- Overall, the results of this study suggest that the passive film stability increased by the repassivation process will be the key importance against the mechanical and electrochemical degradation experienced by dental implants.

**Acknowledgement** The study was funded by NIH (RO3) AR064005 and the University of Illinois at Chicago College of Dentistry. Ducom

Instruments kindly provided the instrument for the tests. Surface analysis was done at Rush University (Tribology lab).

## Compliance with Ethical Standards

**Conflict of interest** On behalf of all authors, the corresponding author states that there is no conflict of interest.

## References

1. Newman M, Takei H, Klokkevold P, Carranza FA (2012) Carranza's clinical periodontology, 12th edn. Elsevier Saunders, St. Louis
2. Nikolopoulou F (2006) Saliva and dental implants. *Implant Dent* 15(4):372–376
3. Jorge JR, Barao VA, Delben JA, Faverani LP, Queiroz TP, Assuncao WG (2013) Titanium in dentistry: historical development, state of the art and future perspectives. *J Indian Prosthodont Soc* 13(2):71–77
4. Ribeiro AL, Hammer P, Vaz LG, Rocha LA (2013) Are new Ti–Nb–Zr alloys potential substitutes of the Ti6Al4V alloy for dental applications? An electrochemical corrosion study. *Biomed Mater* 8(6):065005
5. Mathew MT, Abbey S, Hallab NJ, Hall DJ, Sukotjo C, Wimmer MA (2012) Influence of pH on the tribocorrosion behavior of CpTi in the oral environment: synergistic interactions of wear and corrosion. *J Biomed Mater Res B* 100(6):1662–1671
6. Mathew MT, Uth T, Hallab NJ, Pourzal R, Fischer A, Wimmer MA (2011) Construction of a tribocorrosion test apparatus for the hip joint: validation, test methodology and analysis. *Wear* 271(9–10):2651–2659
7. Sivakumar B, Kumar S, Sankara Narayanan TSN (2011) Fretting corrosion behaviour of Ti–6Al–4V alloy in artificial saliva containing varying concentrations of fluoride ions. *Wear* 270(3–4):317–324
8. Licausi MP, Igual Muñoz A, Amigó Borrás V (2013) Influence of the fabrication process and fluoride content on the tribocorrosion behaviour of Ti6Al4V biomedical alloy in artificial saliva. *J Mech Behav Biomed Mater* 20:137–148
9. Simka W, Sadkowski A, Warczak M, Iwaniak A, Dercz G, Michalska J et al (2011) Characterization of passive films formed on titanium during anodic oxidation. *Electrochim Acta* 56(24):8962–8968
10. Mohedano M, Matykina E, Arrabal R, Pardo A, Merino MC (2014) Metal release from ceramic coatings for dental implants. *Dent Mater* 30(3):e28–e40
11. Nautiyal VP, Mittal A, Agarwal A, Pandey A (2013) Tissue response to titanium implant using scanning electron microscope. *Natl J Maxillofac Surg* 4(1):7–12
12. Farina AP, Spazzin AO, Consani RL, Mesquita MF (2014) Screw joint stability after the application of retorque in implant-supported dentures under simulated masticatory conditions. *J Prosthet Dent* 111(6):499–504
13. Lobbezoo F, Brouwers JE, Cune MS, Naeije M (2006) Dental implants in patients with bruxing habits. *J Oral Rehabil* 33(2):152–159
14. Gao SS, Zhang YR, Zhu ZL, Yu HY (2012) Micromotions and combined damages at the dental implant/bone interface. *Int J Oral Sci* 4(4):182–188
15. Swaminathan V, Gilbert JL (2012) Fretting corrosion of CoCrMo and Ti6Al4V interfaces. *Biomaterials* 33(22):5487–5503
16. Barao VA, Mathew MT, Assuncao WG, Yuan JC, Wimmer MA, Sukotjo C (2012) Stability of Cp-Ti and Ti-6Al-4V alloy for dental

- implants as a function of saliva pH: an electrochemical study. *Clin Oral Implants Res* 23(9):1055–1062
17. Oshida Y (2007) *Mechanical and Tribological Behaviors. Bioscience and Bioengineering of Titanium Materials*. Elsevier, Oxford, pp 105–124
  18. Vieira AC, Ribeiro AR, Rocha LA, Celis JP (2006) Influence of pH and corrosion inhibitors on the tribocorrosion of titanium in artificial saliva. *Wear* 261(9):994–1001
  19. Mathew MT, Barao VA, Yuan JC, Assuncao WG, Sukotjo C, Wimmer MA (2012) What is the role of lipopolysaccharide on the tribocorrosive behavior of titanium? *J Mech Behav Biomed Mater* 8:71–85
  20. Chaturvedi TP (2009) An overview of the corrosion aspect of dental implants (titanium and its alloys). *Indian J Dent Res* 20(1):91–98
  21. Souza ME, Lima L, Lima CR, Zavaglia CA, Freire CM (2009) Effects of pH on the electrochemical behaviour of titanium alloys for implant applications. *J Mater Sci Mater Med* 20(2):549–552
  22. Schiff N, Grosgeat B, Lissac M, Dalard F (2002) Influence of fluoride content and pH on the corrosion resistance of titanium and its alloys. *Biomaterials* 23(9):1995–2002
  23. Nakagawa M, Matsuya S, Shiraishi T, Ohta M (1999) Effect of fluoride concentration and pH on corrosion behavior of titanium for dental use. *J Dent Res* 78(9):1568–1572
  24. Woo Park Y, Sankara Narayanan TSN, Yong Lee K (2006) Effect of fretting amplitude and frequency on the fretting corrosion behaviour of tin plated contacts. *Surf Coat Technol* 201(6):2181–2192
  25. Jauch SY, Coles LG, Ng LV, Miles AW, Gill HS (2014) Low torque levels can initiate a removal of the passivation layer and cause fretting in modular hip stems. *Med Eng Phys* 36(9):1140–1146
  26. Gilbert JL, Mali S, Urban RM, Silverton CD, Jacobs JJ (2012) In vivo oxide-induced stress corrosion cracking of Ti-6Al-4V in a neck-stem modular taper: Emergent behavior in a new mechanism of in vivo corrosion. *J Biomed Mater Res B* 100(2):584–594
  27. Baxmann M, Jauch SY, Schilling C, Blömer W, Grupp TM, Morlock MM (2013) The influence of contact conditions and micro-motions on the fretting behavior of modular titanium alloy taper connections. *Med Eng Phys* 35(5):676–683
  28. Hallab NJ, Messina C, Skipor A, Jacobs JJ (2004) Differences in the fretting corrosion of metal–metal and ceramic–metal modular junctions of total hip replacements. *J Orthop Res* 22(2):250–259
  29. Gil FJ, Canedo R, Padros A, Baneres MV, Arano JM (2003) Fretting corrosion behaviour of ball-and-socket joint on dental implants with different prosthodontic alloys. *Biomed Mater Eng* 13(1):27–34
  30. Manhabosco TM, Tamborim SM, dos Santos CB, Müller IL (2011) Tribological, electrochemical and tribo-electrochemical characterization of bare and nitrided Ti6Al4V in simulated body fluid solution. *Corros Sci* 53(5):1786–1793
  31. Stack MM, Huang W, Wang G, Hodge C (2011) Some views on the construction of bio-tribo-corrosion maps for titanium alloys in Hank's solution: Particle concentration and applied loads effects. *Tribol Int* 44(12):1827–1837
  32. Contu F, Elsener B, Böhni H (2004) A study of the potentials achieved during mechanical abrasion and the repassivation rate of titanium and Ti6Al4V in inorganic buffer solutions and bovine serum. *Electrochim Acta* 50(1):33–41
  33. Runa MJ, Mathew MT, Rocha LA (2013) Tribocorrosion response of the Ti6Al4V alloys commonly used in femoral stems. *Tribol Int* 68:85–93
  34. Barril S, Mischler S, Landolt D (2004) Influence of fretting regimes on the tribocorrosion behaviour of Ti6Al4V in 0.9 wt% sodium chloride solution. *Wear* 256(9–10):963–972
  35. Mischler S, Spiegel A, Landolt D (1999) The role of passive oxide films on the degradation of steel in tribocorrosion systems. *Wear* 225–229(Part 2):1078–1087
  36. Masmoudi M, Assoul M, Wery M, Abdelhedi R, El Halouani F, Monteil G (2006) Friction and wear behaviour of Cp Ti and Ti6Al4V following nitric acid passivation. *Appl Surf Sci* 253(4):2237–2243
  37. Cvijović-Alagić I, Cvijović Z, Mitrović S, Panić V, Rakin M (2011) Wear and corrosion behaviour of Ti–13Nb–13Zr and Ti–6Al–4V alloys in simulated physiological solution. *Corros Sci* 53(2):796–808
  38. Molinari A, Straffelini G, Tesi B, Bacci T (1997) Dry sliding wear mechanisms of the Ti6Al4V alloy. *Wear* 208(1–2):105–112
  39. Stack MM, Abdulrahman GH (2010) Mapping erosion-corrosion of carbon steel in oil exploration conditions: some new approaches to characterizing mechanisms and synergies. *Tribol Int* 43(7):1268–1277
  40. Mischler S (2008) Triboelectrochemical techniques and interpretation methods in tribocorrosion: a comparative evaluation. *Tribol Int* 41(7):573–583

**Publisher's Note** Springer Nature remains neutral with regard to jurisdictional claims in published maps and institutional affiliations.